PCCP

Accepted Manuscript

ROYAL SOCIETY OF CHEMISTRY

www.rsc.org/pccp

Interplay Between Hydrophobic Effect and Dipole Interactions in Peptide Aggregation at Interfaces†

Sai J Ganesan,[a] and Silvina Matysiak*[b]‡

Protein misfolding is an intrinsic property of polypeptides, and misfolded conformations have a propensity to aggregate. In the past decade, the development of various coarse-grained models for proteins have provided key insights into the driving forces in folding and aggregation. We recently developed a low resolution Water Explicit Polarizable PROtein coarse-grained Model (WEPPROM) by adding oppositely charged dummy particles inside protein backbone beads. With this model, we were able to achieve significant α/β secondary structure content, without any added bias. We now extend the model to study peptide aggregation at hydrophobic-hydrophilic interfaces and draw comparisons to aggregation in explicit water solvent. Elastin-like octapeptides $(GV)_4$ are used as a model system for this study. A condensation-ordering mechanism of aggregation is observed in water. Our results suggest that backbone interpeptide dipolar interactions, not hydrophobicity, plays a more significant role in fibril-like peptide aggregation. We observe a cooperative effect in hydrogen bonding or dipolar interactions, with increase in aggregate size in water and interface. Based on this cooperative effect, we provide a potential explanation for the observed nucleus size in peptide aggregation pathways. The presence of a hydrophobic-hydrophilic interface both (a) increases order of aggregates formed, and (b) rate of aggregation process. Without dipolar particles, peptide aggregation is not observed at the hydrophilic-hydrophobic interface. Thus, the presence of dipoles, not hydrophobicity plays a key role in aggregation observed at hydrophobic interfaces.

1 INTRODUCTION

Elongated protein fibrils are associated with multiple neurological diseases, such as Alzheimer's, Huntington's and prion diseases, among others [1–3]. Studies also suggest that the ability of proteins and peptides to form amyloid fibril structures is not limited to disease conditions, but a generic property of polypeptides [4–6]. The "core structure" of mature amyloid fibrils is known to involve an alignment of short peptide segments, between 6 and 12 residues, into cross-β structures [7]. Many kinetic mechanisms of aggregation have been proposed [8], however, nucleation-growth process [9,10] is the more accepted and dominant view. In the nucleation-growth process, a lag phase is observed, during which a nucleus (or a small oligomeric aggregate) is formed, followed by the rearrangement and elongation of the nucleus to fibrillar or ordered structures, known as the growth phase. Studies have revealed a number of potential intermediate species that can either lie on- or off-pathway to aggregation [11–13], thus suggesting the existence of a number of pathways to the final aggregated state.

The exact nature of the "nucleus" is not known, however, the presence of disordered aggregates seem to appear as intermediate states in many cases, and have been suggested to play the role of an "initiation site" for ordered amyloid fibril growth [10,14,15]. A condensation-ordering mechanism, where a disordered oligomer is formed initially, which eventually aligns to form a more ordered structure, has been observed in many experimental and theoretical studies of amyloid formation [3,10,16–18]. The common β-sheet structured core, seen in ordered fibrils formed by various polypeptides, suggests that intermolecular backbone hydrogen bonding is critical for the assembly of amyloid fibrils [19]. While hydrophobic interactions are crucial in stabilizing native proteins, the backbone hydrogen bonding network is known to be a dominant force in stabilizing amyloid fibrils [20,21]. The cooperativity of this hydrogen-bond network, observed from first principle calculations, is believed to provide an extra-stabilization to peptide fibrils [22,23].

The presence of surfaces such as cellular membranes is emerging as an important factor in amyloid formation, especially in the context of *in vivo* biological systems [24]. Solid surfaces have been observed to influence protein aggregation kinetics and morphology in a variety of peptides [25,26]. Confinement to two dimensions leads to an enhancement of protein concentration, whereas surface interactions promote the formation of aggregation-prone structures via an ordered templating mechanism. Aggregation studies on spherical nanoparticles revealed a condensation-ordering mechanism, similar to what was observed without a surface, independent of hydrophobicity [14,27]. Experimental studies also suggest changes in conformation and hence aggregation morphologies, induced by the presence of surfaces [28]. In fact, octapeptides have been extensively studied using experiments [29–33].

Water-hydrophobic interfaces have been used as a model system to understand peptide aggregation on membranes. In particular, hexadecane slabs are known to be a good membrane mimetic environment [34]. Experimental and simulation

0† Electronic Supplementary Information (ESI) available:
0[a] *Department of Bioengineering, University of Maryland, College Park, Maryland, USA.*
0[b] *Department of Bioengineering and Biophysics Program, University of Maryland, College Park, Maryland, USA. Tel: 301 405 0313; E-mail: matysiak@umd.edu*

studies have shown $(GV)_n$ peptides to be good models for studying amyloid formation, as these peptides have a propensity for forming β-sheet containing fibrils, both in water and at octane-water interfaces[35,36]. Here, we use molecular dynamics simulations (MD) with a coarse-grained peptide model to investigate how dipole interactions and interfaces can influence self-assembly of ordered peptide aggregates. Coarse-grained (CG) models have made a huge impact on our understanding of how peptides/proteins aggregate in scales difficult to achieve by atomistic simulations[37–39]. While atomistic simulations have given us insights into the first aggregation steps, they are unable to capture the entire aggregation process from monomeric species to fibrillar species[40,41]. Most on- and off-lattice CG models that successfully capture different aspects of the oligomerization process renormalize the solvent environment through effective short-range, inter-residue interactions and do not take into account dipolar interactions[42–46]. We recently proposed a new water-explicit off-lattice CG protein model, which we now call WEPPROM (Water-Explicit Polarizable Protein Model)[47]. WEPPROM has roots in the MARTINI force field[48]. WEPPROM models a protein backbone bead with a flexible dipole, thus introducing structural polarization. The inclusion of backbone dipoles allows the protein model to achieve *de novo* helix and sheet content, based on the primary sequence, without any biases. We found that dipolar interactions contribute to cooperativity in folding secondary and supersecondary structures. Since hydrogen bonds are a type of dipole-dipole interactions, these added dipoles mimick Hydrogen-bond (H-bond) effect. However, it is important to stress on the fact that H-bonds have a covalent character due to the involvement of orbital interactions, which contributes to the directionality of the hydrogen bond[49,50]. In water, the hydrogen bond is known to be roughly 90% electrostatic and 10% covalent in nature[51]. Since peptide backbone hydrogen bonds are also weak in nature, we think modeling H-bonds as dipole-dipole interactions is a reasonable approximation.In this work, we have used this new CG polarizable model to probe the role of dipole interactions and water-hydrophobic interfaces in the aggregation of $(GV)_4$ octapeptides into fibril-like structures. Since in the WEPPROM model, the backbone dipole can fluctuate, we characterize if backbone dipoles exhibit any cooperative effect upon peptide aggregation, and how that translates to the stability and formation of fibril-like peptide aggregates. We investigate the balance between hydrophobic effect and dipole interactions in water and at interfaces. Our results suggest a difference in this balance for aggregation in water and at the interface. That is, hydrophobicity plays a more significant role for aggregating peptides in aqueous solution than at hydrophobic-hydrophilic interfaces. At hydrophobic-hydrophilic interfaces, without backbone dipolar particles, peptide aggregation is not observed.

2 METHODS

Table 1 List of Simulations

System	Peptides	Concentration (M)	Runs	Interface
I	2	0.025	8	No
II	3	0.0375	8	No
III	4	0.05	8	No
IV	8	0.075	8	No
V	12	0.15	8	No
VI	12	0.15	8	Yes

2.1 System Setup

The block octapeptide $(GV)_4$ was modeled as a repeat neutral (N) and hydrophobic residue (H) sequence, respectively (see Figure 1a). The neutral residue was modeled as a spherical polar backbone bead (BB), which has an embedded dipole, as shown in Figure 1b. The hydrophobic residue has a hydrophobic side chain (SC) bead, in addition to the backbone bead.

The backbone coarse grained bead consists of three interaction sites, the center bead BB, and two dipole particles, BBm and BBp. The main site, the center of the BB bead, interacts with other CG beads through a pairwise Lennard-Jones (LJ) potential. Dipole particles BBm and BBp are harmonically bound to the central particle BB (equilibrium distance (l), force constant (k_l)), and carry a positive and negative charge of equal magnitude (q), respectively. These dipole particles interact with other particles via electrostatic interactions. An harmonic angle potential (equilibrium angle (θ) and angular force constant (k_θ)) was used to control the rotation of BBm and BBp particles. For solvation, a polarizable CG water model was used[52]. Since the location of the dipole particles were not fixed, the model is polarizable. That is, changes in dielectric medium or local environment, results in induced backbone dipoles and hence structural changes. This makes WEPPROM model suitable for this study. Details on parameterization methods and forcefield parameters are provided in reference 1.

A hexadecane molecule was modeled as 4 hydrophobic beads, using 1:4 mapping scheme, with a backbone bond length of $0.47nm$ (bond constant $k_l = 1250kJ/mol$); angle of θ=180° (angle constant $k_\theta = 25kJ/mol$), taken from the MARTINI forcefield[48]. The pairwise LJ interactions for these hydrophobic beads is the same as that for the hydrophobic side chain bead used in WEPPROM.

2.2 Simulation Parameters

Peptide concentrations along with assigned system names used in this study are reported in Table 1. A cubic box of 5nm length with water density of $1040 kgm^{-3}$ was used for simulations in explicit water. For simulations with hexadecane or an interface, a rectangular simulation box of equivalent volume of water and hexadecane (density $1090 kgm^{-3}$) in a 5x5x10nm dimension was used. Both densities were obtained from equilibrium NPT simulations at 300K temperature and 1atm pressure respectively[52]. Snapshot images of initial system setup are shown in Figure S1. Eight replicate simulations of each concentration system were performed with the NVT ensemble at T=300K. To study the effect of temperature, eight replicate simulations of 12 peptide system in water was run at temperatures 350K, 365K, 375K, 385K and 400K.In each replica, distinct initial conformations of the peptides were assigned using a different set of random seeds. The highest concentrated system (12 peptide/system V), was studied in the presence of a water-hexadecane interface (system VI), keeping the concentration in water constant. To explore the role of sequence, we also looked at 12 poly-glycine (polyG) and poly-valine(polyV) octapeptides, both at the interface and in aqueous solution. These simulations were performed at 300K. To characterize the role of dipolar interactions, a set of control runs of system V and VI, without dipolar particles were also carried out. A total of 100ns data was collected for each system. All simulations were carried out using the GROMACS package[53] version 4.5.5, and visualized on VMD[54]. Nose-Hoover thermostat (time constant=1ps) was used to keep the temperature at 300K. A time step of 5fs was used in all the simulations, and the neighbor list was updated every 10 steps. The long-range electrostatic interactions with periodic boundary conditions (xyz) were calculated by the particle-mesh Ewald method[55]. A global dielectric constant of 2.5 was used. The LINCS algorithm[56] was used to constrain the bonds of the water molecules (between the central CG site and the dipole particles).

2.3 Analysis

The last 50ns of each trajectory was analyzed, unless otherwise stated.

2.3.1 Order Parameter. Dipole order was evaluated using the principal method for determining orientational order in liquid crystalline systems, or the P2 order parameter[57]. This order parameter is given by $\frac{3}{2}\lambda_{max}$, where λ_{max} is the highest eigenvalue of matrix S_d (Equation 1). N is the total number of backbone beads, u_i is a unit dipole vector within a backbone bead. P2 is 1 for a fully ordered system and 0 for a random system[58].

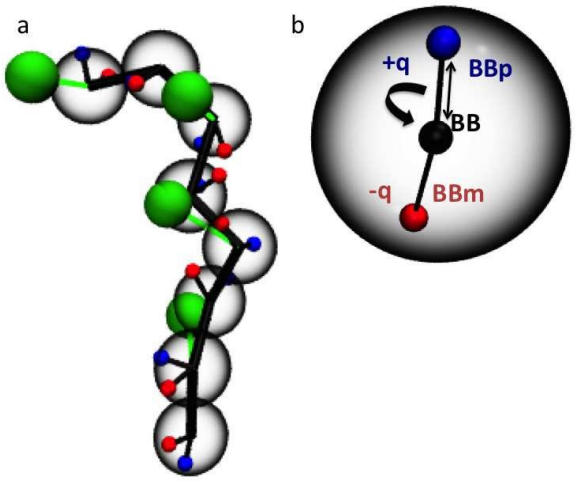

Fig. 1 (a) Coarse-grained representation of $(GV)_4$ peptide, backbone beads (BB) are represented in translucent black, hydrophobic side chain beads in green, and positively and negatively charged dummies in blue and red respectively. (b) Polarizable BB bead; vdW radius of BB bead encloses dummy particles, BBm (negatively charged) and BBp (positively charged).

$$S_d = \frac{1}{N}\sum_i \begin{pmatrix} u_i^x u_i^x - \frac{1}{3} & u_i^x u_i^y & u_i^x u_i^z \\ u_i^y u_i^x & u_i^y u_i^y - \frac{1}{3} & u_i^y u_i^z \\ u_i^z u_i^x & u_i^z u_i^y & u_i^z u_i^z - \frac{1}{3} \end{pmatrix} \quad (1)$$

Peptide order was also calculated using the above P2 parameter, with N as the total number of peptides, and u_i as the end-to-end vector ($\vec{R}$) of a peptide. A similar definition of the orientational order parameter to characterize peptide aggregation has been used in a number of aggregation studies[46,59,60].

2.3.2 Dipole Moment and Energy. Dipole moment (μ) for each backbone bead, in an aggregate, was evaluated using Equation 2. The quantities r_{BBm_i}, r_{BBp_i}, q_{BBm}, q_{BBp} represent position vectors and charge of the two dummy particles, and r_{com_i} is the center of mass vector of the backbone bead.

$$\mu_i(r_i) = q_{BBm}(r_{BBm_i} - r_{com_i}) + q_{BBp}(r_{BBp_i} - r_{com_i}) \quad (2)$$

2.3.3 Pseudo Hydrogen Bonds. Since hydrogen bonds are a type of dipole-dipole interactions, and WEPPROM models a peptide backbone (CO-NH) as a dipole, we refer to dipolar interactions in our model as "pseudo" hydrogen bonds (H-bond). WEPPROM models H-bonds as purely dipole-dipole interactions and does not account for the covalent character of H-bonds. This is also the reason we refer to dipole-dipole interactions as "pseudo" H-bonds. The number of interpeptide pseudo hydrogen bonds was calculated as a measure of

sheet content. A H-bond was defined between any two oppositely charged dummy particles on distinct peptides, within a cut-off of 2.5Å. This cut-off corresponds to the peak of a pairwise distance distribution between positively and negatively charged dummy particles in helical (*i* and *i+4*) and sheet conformations (see Figure S2a).

2.3.4 Water Expulsion. To explore the role of solvent, we evaluated the number of water molecules around hydrophobic side chain beads. We used a cut-off of 6.6 Å, which corresponds to the location of the first minima in the radial distribution function (RDF) plot between water and hydrophobic side chain beads (Figure S2b).

2.3.5 Conformational Analysis and Kinetics. Aggregates formed can either be disordered or ordered β-sheets. Conformations were classified using the following criteria: if a peptide in an aggregate, made less than two pseudo interpeptide hydrogen bonds with any other peptide, it was classified as a monomer (M), else, defined as part of an aggregate. If each peptide of the aggregate made at least $\frac{n}{2}$ H-bonds, where n is the length of the peptide, we termed the aggregate as an ordered aggregate, else, intermediate or disordered. This criteria is consistent with a similar kinetics study from Hall's group on peptide aggregation[61]. We used the same criteria for our temperature studies as well. To compare kinetics or dynamics of aggregates between systems, with and without dipolar particles, a backbone bead cutoff (5Å) was used in place of interpeptide H-bonds. This cutoff was obtained by comparing pairwise distance distributions between backbone beads of different peptides in an aggregate, with and without dipolar particles, for 12 peptides system V (blue and red curves in Figure S2c).

The ordered aggregates can either adopt a "cross-β" or "fibril-like" conformation in water. Radius of gyration (R_g) was used to distinguish these two ordered populations. As shown in Figure S3a and S3b, a "cross-β" like aggregate populates the $\frac{R_g}{\sqrt{N}}$ (where N is the number of peptides) region of 1.5 to 2.5nm and has at least 6 inter-peptide H-bonds. Whereas a "fibril-like" aggregate occupies the region of 3.5 to 4.5nm and has greater than 8 inter-peptide H-bonds. The above parameters were used to determine the conformational frequency of $(GV)_4$ aggregates in water. At the interface, only "fibril-like" aggregates were seen, and hence the H-bond cutoff was sufficient to distinguish ordered from disordered conformations.

2.3.6 Potential Mean Force. Potential mean force (PMF) for aggregates in water and at the interphase, for systems with and without dipoles were evaluated using Equation 3. The quantities $p(R_g)$ is the probability distribution of radius of gyration of the aggregate formed, W is the PMF, k_b is the Boltzmann constant and T is 300K in our study.

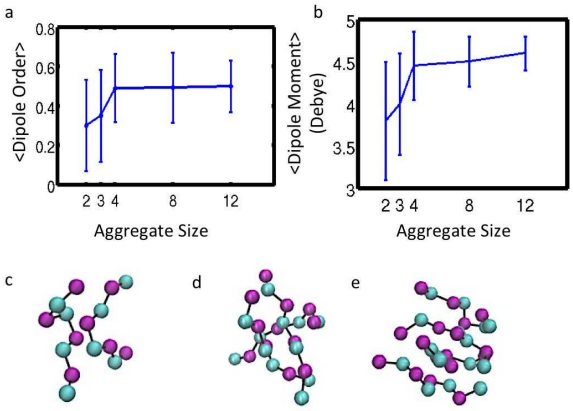

Fig. 2 Average (a) dipole order and, (b) dipole moment per backbone bead with respect to $(GV)_4$ aggregate size. All error bars represent 95% confidence interval for the mean (assuming normal distribution) of collective data, as standard error of the mean is negligible due to large number of conformational information collected. Representative conformation of (c) 2 peptide aggregate; (d) 3 peptide aggregate; and (e) 4 peptide aggregate. Cyan and purple beads correspond to backbone representation of hydrophobic and neutral residues respectively.

$$W(R_g) = -k_b T ln p(R_g) \tag{3}$$

3 Results and Discussion

3.1 Effect of Concentration

We first present the results characterizing the effect of concentration in determining the structure and stability of aggregated conformations. All the simulations performed in explicit water resulted in transient or stable aggregate structures.

To characterize the conformations, we looked at the time evolution of the average backbone dipole moment (Figure S4). Backbone dipole moments of 2 and 3 peptides systems (I and II) fluctuate between 3 and 5D (Figures S4a-b), whereas, for systems III and IV (4 and 8 peptides systems), the value remains constant at around 4.5D after 10ns (Figures 4c-d). System I (2 peptides) fluctuates more than system II (3 peptides), and system II stabilizes higher dipole moment conformations. Therefore, more ordered and stable conformations are observed in system II, at 300K. Whereas, aggregates of 4, and 8 peptides result in stable, structured and ordered conformations. Figures 2c-e are representative conformations of 2, 3 and 4 peptide aggregates, respectively.

These results lead us to the following question: why is the 4 peptide aggregate, the smallest, stable, ordered aggregate? To answer this question, a few backbone(BB) dipole parameters

were evaluated. The BB dipole order, and BB dipole moment per residue of various aggregate conformations are depicted in Figure 2a and 2b, respectively. The dipole moment and order exhibit a sharp increase from an aggregate size of 2 to one of size 4. Adding more layers of peptides to an aggregate of size 4 does not significantly increase the dipole order or moment per residue. Specifically, the dipole moment can be considered as a representative strength of the pseudo hydrogen bond network. From Figure 2b, we see an increase in this strength up to four layers of peptides, before leveling off at 4.5 D. That is, there exists "cooperativity" in both dipole order and moment with increase in aggregate size, that saturates at aggregate size 4. This cooperativity of pseudo hydrogen bonds or dipolar interactions contributes to the stability of the four peptide aggregate. Therefore, an aggregate of size 4 is the minimum aggregate size with the highest dipole moment per residue. This size coincides with previous studies that have identified a nucleus size for aggregation between 3 and 4 peptides[62]. Cooperative effect of hydrogen bond networks in amyloid fibrils has been previously studied using *ab initio* calculations. A DFT study on peptide GNNQQNY from yeast prion Sup35, also identified a nonlinear increase in energy per monomer, up to 4 layers of peptide, before saturation[23]. A similar effect caused by side chain hydrogen bonding of polyQ aggregates has also been observed[22].

Dipole energy, which is a measure of how aligned a dipole vector is to the local electric field (E), given by expression $< -\vec{\mu}.\vec{E} >$ was also evaluated[47,63]. Figure S5a depicts the dipole energy per peptide with respect to aggregate size, and shows a linear increase in dipole energy with aggregate size (a linear fit is shown in red). The observed linear increase is due to the local electric field strength, which increases with aggregate size. The angle between the backbone dipole vectors and the local electric field is shown in Figure S5b. This angle is a measure of the alignment between backbone dipole vectors and the electric field. A decrease of this angle with aggregate size is due to a better alignment with the local electric field. It is interesting to note that this decrease in alignment also saturates at an aggregate size of 4, thus revealing a cooperative behavior consistent with dipole moment and dipole order (Figures 2a and 2b).

3.2 Energetic Contributions and Role of Water

As shown in Figure 3, within 5ns, randomly distributed peptides collapse into disordered aggregates with the formation of a hydrophobic core for system V (12 peptides). This disordered aggregate then rearranges to form either "fibril-like" or "cross-β" like sheet structures. These results indicate a two-step condensation-ordering mechanism, that has previously been identified in simulations of $A\beta_{16-25}$, $A\beta_{25-35}$, prion protein Sup35 and capped polyalanine sequences[10,43,64]. In this

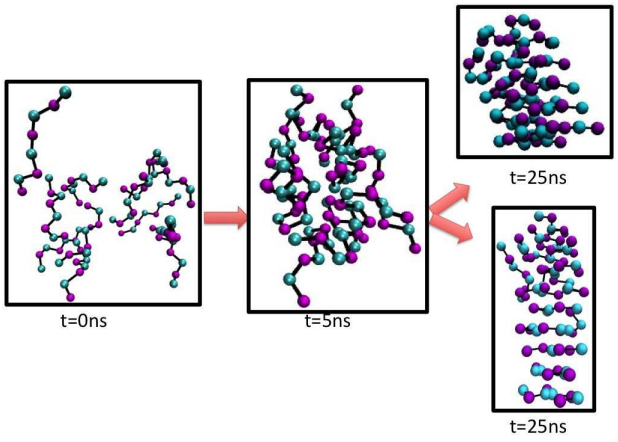

Fig. 3 Observed aggregation mechanism for $(GV)_4$ peptide in water. Initial conformation of system V (12 peptides with backbone representation) at 0ns; disordered aggregate formed at around 5ns. Inset shows the presence of a hydrophobic core. Ordered aggregates formed at 25ns adopt "cross-β" like (top) or "fibril-like" (bottom) conformations. Cyan and purple beads correspond to backbone representation of hydrophobic and neutral residues respectively. Hydrophobic side chain beads shown in green.

mechanism, a disordered oligomeric aggregate structurally reorganizes into ordered amyloid fibrils[27].

We take a closer look at peptide-peptide energetic contributions to identify the driving forces behind the aggregation process. The time evolution of LJ hydrophobic side chain interactions (red curve), backbone Coulombic interactions (black curve), and total interpeptide energy (blue curve) for representative trajectories are shown in Figures S6a-e, for different peptide systems. These energies are normalized by the number of peptides in the aggregate. These plots clearly indicate that the initial conformation of randomly distributed peptides has the highest energy (Figures S6c-e), except in the 2 and 3 peptide systems (Figures S6a-b), where the aggregates formed are neither stable nor ordered. The transient nature of 2 and 3 peptide aggregates is visible from the transitions seen in energy values (Figures S6a-b). However, for the remaining systems, the final aggregate is the conformation of lowest energy. It is interesting to note that the trend followed by the total peptide-peptide energy (blue curve) is similar to the Coulombic energy (black curve) in systems II (3 peptides), III (4 peptides), IV (8 peptides) and V (12 pepdise), see Figures S6b-e. The Coulombic energy displays the largest energy drop in these systems. This drop in energy arises from backbone dipolar interactions, or interpeptide hydrogen bonds. For systems III, IV and V (4, 8 and 12 peptides, see Figures S6c-e), the Coulombic and total peptide energy decrease until 20ns, and remains constant thereafter, till the final aggregate conformation is reached. A comparison of representative hydrophobic side chain interac-

tions for the above described systems are shown in Figure S6f. For aggregates of size 8 and 12 (blue and black curves respectively), the hydrophobic contribution is comparable and more drastic than for smaller aggregates of size 2 (red), 3 (pink), and 4 (green). This is because the largest drop in hydrophobic LJ energies is due to the formation of a hydrophobic core, which is not formed in the case of smaller aggregates. A control run of 12 peptide system V without dipoles, exhibits hydrophobic collapse and results in disordered structures (discussed later). Therefore, interpeptide hydrogen bonding plays a major role in driving ordered structures. This is in agreement with many studies that have suggested a larger role for backbone hydrogen bonding than hydrophobic interactions in amyloid fibril aggregation[14,21,27,65]. Gordon *et.al.* showed that replacing two amide bonds of $A\beta_{16-20}$ with ester groups lacking amide protons prevented aggregation, thus shedding light on the relevance of backbone interpeptide hydrogen bonding, even for a largely hydrophobic peptide.

We also looked at water expulsion from the first hydration shell of hydrophobic side chain beads (N_w). In most of the trajectories (63.5%), a large drop in N_w is observed prior to the increase in pseudo-hydrogen bonds N_{hb} (Figure S10a). The initial large drop in N_w signals a fast hydrophobic collapse of the peptides into an amorphous aggregate. That is, water expulsion from the side chains precedes interpeptide backbone hydrogen bonding. The observed process is similar to the proposed two-step mechanism for amyloid formation by Thirumalai *et.al*[66]. In this proposed mechanism, akin to protein crystallization, water expulsion from the hydrophobic core occurs prior to conformational rearrangement. We observed three other mechanisms, they are: (a) total coupling of water expulsion with structural ordering. That is, there is an increase in water expulsion (or decrease in N_w) with increase in pseudo H-bond content with time; (b) partial and initial coupling of water expulsion with structural ordering. There is an increase in water expulsion with increase in pseudo H-bond content only in the first few ns; and (c) stepwise water expulsion, which is observed when "fibril-like" conformations are formed. There is an initial expulsion when the aggregate is initially formed, and another when it becomes more ordered. A detailed description of this mechanism can be found in the supplementary material under the section Mechanisms of Water Expulsion.

3.3 Effect of Water-Hydrophobic Liquid Interface

Figure 4 compares the conformational frequency between 12 peptide systems (a) in water (system V, blue bars), (b) in the presence of a hydrophobic interface (system VI, green bars) and (c) without dipolar particles (red bar). The presence of a hydrophobic surface influences aggregation morphology by shifting the conformational equilibrium. In water, two distinct

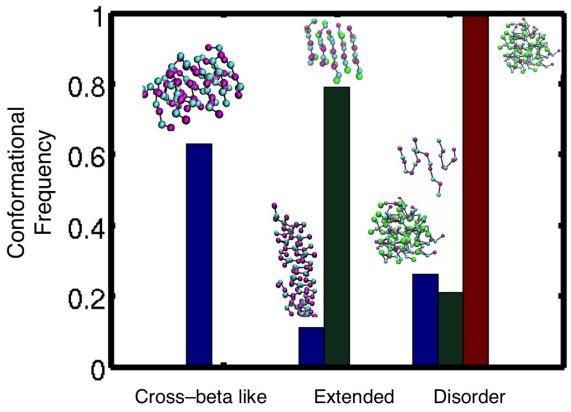

Fig. 4 Conformational frequency of 12 peptides system V (blue), VI (green), and control system without dipolar particles in a water environment (red). Representative conformations are shown as insets, backbone beads represented in cyan (hydrophobic residue) and purple (neutral residue). Hydrophobic side chain beads shown in green.

types of conformations are seen, (a) a cross-β like conformation with a frequency of 0.6, and (b) an extended fibril-like conformation, with a frequency of 0.1. Both conformations are seen with 12 and 8 peptides. Studies on $A\beta_{1-40}$ show that within 6-10 monomer chains, cross-β like order is seen[67]. The "fibril-like" conformation is more water exposed (red curve in Figure S2b) than the "cross-β-like" conformation (blue curve in Figure S2b), as evident from the RDF between water and hydrophobic side chains beads. We refer to the dominant closed conformations as "cross-β-like" as they are a pair of ordered β-sheets with side chains of the two sheets interdigitated in a dry hydrophobic core (see Figure S7d, Figure 3 and Figure 6)[68,69]. These structures are similar to the MVGGVV microstructure crystallized by Eisenberg's group[70].

With the presence of a hydrophobic surface there is a conformational shift to "fibril-like" structures, with the hydrophobic beads partitioning into the hexadecane phase (Figure 7c). The frequency of ordered, extended conformations in the presence of an interface is 0.8. Another important feature is the decrease in disordered conformations by about 10% in the biphasic system compared to bulk water. The disordered conformations seen at the interface are smaller in size, consisting of 3 or less peptides, as the peptides can interact with two water-hexadecane interfaces (see Figures S1). Partitioning of valine or hydrophobic residues into hexadecane restricts or constrains the peptides to two dimensions. This restriction increases the probability of peptides colliding as the local concentration increases, which can in turn lead to an increase in peptide-peptide hydrogen bonds and hence, aggregation. Insets in Figure 4 show representative conformations.

Figure S7a shows the difference in order parameter P2 for

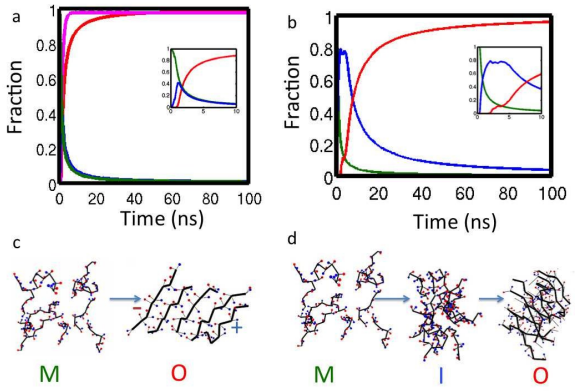

Fig. 5 Time evolution of the fraction of different species in 12 peptides system (a) VI and (b) V. Green represents monomer fraction; blue, intermediate aggregate fraction, pink is a negative exponential fit and red, ordered aggregate conformation. (c) Representative pathway for ordered aggregate formation at hydrophobic-water interface, monomers [M] form ordered aggregates [O] with shortly lived intermediates. (d) Representative pathway for ordered aggregate formation in explicit water, monomers [M] form intermediate aggregates [I] which rearrange to form ordered conformation [O].

aggregates in water ($\langle P2\rangle$=0.48) and in the presence of an interface ($\langle P2\rangle$=0.65). The "fibril-like" conformations seen in water are slightly more ordered ($\langle P2\rangle$=0.52, red point in Figure S7a) than the average, however, the presence of an interface results in a significant increase in P2 values. Surface adsorption of the peptide enhances order, as has also been observed in atomistic studies of $(GV)_4$ [36,71,72]. The presence of a surface can lower the entropic penalty to form an ordered state. As shown in Figure S7b, Figure S12 the fibril-like conformations, both in water and at interface, exhibits Pauling and Corey's α-sheet structure [73]. All the negatively charged dipole particles are oriented on one side of the sheet, with all the oppositely charged ones aligned on the other side, as shown in Figure S7b. The alignment of the dipoles is denoted by green arrows in Figure S7b. This distribution of partial charges from the peptide backbone, creates a distinct molecular dipole. α-sheets or "polar pleated sheets" have not received much attention since it is rare in crystal structures. However, recent studies suggest the possible involvement of α-sheets in early stages of amyloidosis [74,75].

3.4 Kinetics and Mechanism of Aggregation

A comparison of kinetic properties of aggregation in water and the more probable aggregation pathway in biphasic systems is depicted in Figures 5a-b (another set of trajectories is represented in Figure S8). Based on the insets of Figures 8a-b (red curves), the "lag phase" which precedes ordered aggregation is more prominent in water ($\approx$ 3ns) than in the presence of an interface ($\approx$ 1ns). In water, the monomers (M) (green curve) aggregate to form an intermediate disordered state (I) (blue curve), which after 25ns, reorganizes to form ordered sheets (O) (red curve). Representative conformations are shown in Figure 5d. Whereas, when the water-hexadecane surface is present, the monomers form sheets in less than 10ns (see red curve). Even though there is an intermediate conformation present, as expected from Figure S12, this state is short lived in comparison to the intermediate conformation observed in water (see blue curve of Figure 5a inset). The nature of the ordered fraction curves (red) is more exponential in the biphasic system (negative exponential fit shown in pink in Figure 5a) than in water, implying a more cooperative process. Representative conformations are shown in Figure 5c, note the "α-sheet" like final conformation. Thus the presence of the water-hydrophobic interface, aids or accelerates the rate of sheet formation, relative to water, as has been observed experimentally [76].

At 300K, we see unidirectional progression of aggregation, thus the mechanism is downhill. As one might expect, ordered aggregation is dependent on temperature. Figure S9 represents average (over 8 runs) monomer (green curve), disordered aggregate (blue curve) and ordered aggregate (red curve) fraction at different temperatures of system V. Aggregates formed are stable and ordered till 350K. This is consistent with other simulation results that show a range of temperatures over which fibrils are formed [77,78]. However, on further increase in temperature, the probability of observing ordered aggregates drops, and is 0 at 400K, with 375K being the transition temperature. At high temperatures, the probability of observing stable aggregates drops [79].

Figure S9a and b represent kinetic properties of aggregation in water (solid lines) and at interface (dashed lines), for polyG octapeptides (Figure S9a) and polyV octapeptides (Figure S9b). In the case of polyG, the monomer fraction stays at 1 throughout the 100ns simulation (green curve in Figure S9a). Therefore, polyG octapeptides do not aggregate in water as backbone dipoles of glycine residues prefers to interact with water. Since glycines are neutral, when a hydrophobic interface is present the peptides do not partition to the hydrophobic interface, and hence do not aggregate at the interface either. In the case of polyV octapeptides in water, a disordered aggregate is formed within the first 10ns (blue solid curve in Figure S9b), however, the fraction of ordered aggregate (red solid curve in Figure S9b) does not significantly increase with time and converge at a fraction of 0.23. For polyV octapeptides at the interface, there is partitioning of the hydrophobic side chains within the first few ns, and the peptides diffuse to form fully ordered conformations within the first 20ns (dashed red curve in Figure S9b). This behavior of polyV octapeptides at

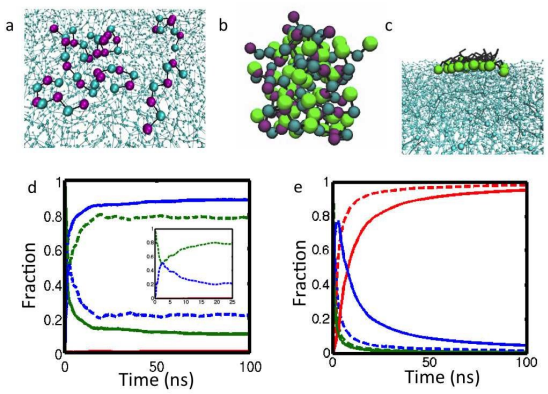

Fig. 6 Representative conformations of 12 peptides system (a) VI and (b) V without dipolar particles. Cyan and purple beads correspond to backbone representation of hydrophobic and neutral residues respectively. Hydrophobic side chain shown in green. (c) Partitioning of hydrophobic side chain beads (green) to the hexadecane phase (cyan) for system VI with dipolar interactions. Peptide backbone shown in black. Time evolution of the fraction of different species, using the backbone distance cutoff in (d) system VI (dashed lines) and system V (solid lines) without dipolar particles, and (e) system VI (dashed lines) and V (solid lines) with dipole particles. Green represents monomer fraction, blue, intermediate aggregate fraction and, red, ordered aggregate.

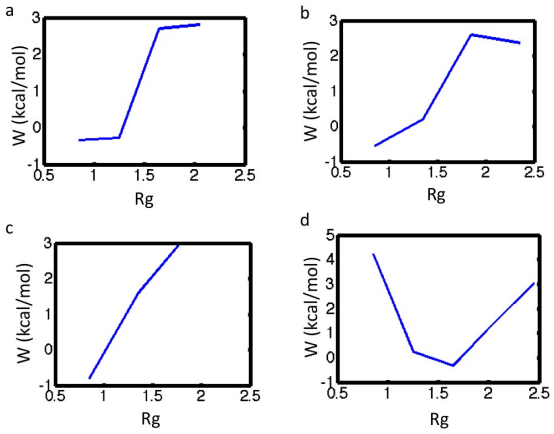

Fig. 7 PMF as a function of the peptide aggregate radius of gyration (Rg). PMF for peptides with dipoles (a) in explicit water and (b) at the interface; and peptide aggregates without dipoles (c) in explicit water and (d) at the interface. All represented ensembles obtained at 300K.

interface is similar to that of GV_4.

3.5 Role of Dipole Interactions

To further investigate the role of dipolar interactions, systems V and VI (12 peptides system with and without interface, respectively) were simulated without dipolar particles. In water, the peptides aggregate due to the hydrophobic effect, however, the aggregates are disordered owing to a lack of pseudo interpeptide H-bonds. A representative collapsed conformation is shown in Figure 6b. To quantify the aggregation pathway, we estimate kinetic parameters using backbone bead cutoffs (see Methods section). This cutoff is defined because the control systems do not have dipole particles, and hence lack interpeptide pseudo hydrogen bonds.

As can be seen from Figure 6d, the monomers (solid green curve) interact to form disordered aggregates (solid blue curve). Since there are no dipolar interactions, there is no order in the aggregate. The ordered conformational fraction remains at 0 (solid red curve). To compare this control run with system V, the same criteria, and cutoff is applied to a representative replicate where dipole interactions are taken into account. Figure 6e (solid curves) displays a similar trend as seen in Figure 6b (discussed above) for the bulk water environment. That is, the monomers aggregate within a few ns to form a disordered aggregate, which in turn rearranges to form ordered aggregates after 25ns.

In the presence of an interface, the peptides(without dipolar interactions) get adsorbed to the surface, due to partitioning of hydrophobic side chains. Representative conformations are shown in Figures 6a and 6c. However, due to the lack of interpeptide dipole interactions, the peptides do not aggregate on the interface, and are free to diffuse individually. Since the hydrophobic side chain can partition to hexadecane, the entropy is driving the peptides to not aggregate. Based on this, we conclude that at hydrophobic interfaces, the major driving force for peptide aggregation is dipolar interactions, which in our model mimics hydrogen bonding. Figure 6d (dashed lines), further elucidates this point. The monomer fraction (green dashed curve) decreases as the peptides aggregate and reach the interface, however, there is an increase soon after 5ns (see inset of Figure 6d). This is due to the fact that the monomers without dipolar particles, on reaching the interface, are free to diffuse. Since the hydrophobic side chains remain buried in hexadecane there is no other driving force to keep the peptides aggregated. Whereas, system VI, that contains dipolar interactions (see Figure 6e), forms an ordered aggregate (dashed red line) within the first 10ns.

To further quantify these processes, we looked at PMF (W) of peptide aggregates with respect to R_g. Figures 7a-b represents PMF of systems with dipoles in water and at the interface, respectively. Both these systems display clear minima for lower values of Rg (Rg $<$1nm), which correspond to ordered aggregates. These curves also display a sigmoidal trend, consistent with cooperative processes. Figures 7c-d represents PMF of systems without dipoles in water and at the interface respectively. Figure 7c clearly shows a minimum corresponding to the aggregated state (Rg $<$1nm), this corresponds to the

disordered state originating from a hydrophobic collapse (see Figure 6b). Whereas, Figure 7d shows a minimum for states with larger Rg (Rg >1.5nm), as these peptides do not form aggregates (see Figure 6a).

4 Conclusion

In this study, we have used WEPPROM to study peptide aggregation of $(GV)_4$ octapeptides. Many of our results are concurrent with all-atom aggregation studies on $(GV)_4$. For example, in all-atom studies, kinetics and mechanism of aggregation at biphasic interfaces (octane-water) are observed to be different than in aqueous solvent[36]. The preliminary step for β-sheet formation at octane-water interfaces is also the initial partitioning of non-polar side chains. The adsorbed peptides diffuse in 2D before forming intermolecular hydrogen bonds, that brings order to the aggregates. Both hairpin-like and fully extended conformations are observed on the interface and in water. All of which are observed in our study. However, in atomistic studies, not all peptides that adsorb to the surface form aggregates. This is due to a time lag in peptide diffusion as all-atom studies are limited by time scale. From our CG studies, we have been able to observe a difference in balance between hydrophobic and backbone dipole-dipole interactions, between amphipathic aggregating peptides in water and at a hydrophobic interface. The dipole interactions plays a more significant role in driving aggregation at interface.

We observe a cooperative effect in interpeptide pseudo hydrogen bonding with aggregate size, that stabilizes at aggregate size 4. That is, the backbone dipole moment and order increases non-linearly up to 4 layers and then levels off. These dipole interactions, within the β-strands are cooperative, with contributions from several layers away within the ordered aggregate. The backbone dipoles get aligned with the aggregate electric field up to 4 peptide layers, where it levels off at 40 degrees. That is, the tetrameric GV_4 species is the smallest, stable aggregate that has the highest backbone dipole moment. Studies on Amyloid-β oligomers, have also identified trimeric and tetrameric species to be stable, long-lived oligomers that might play a role in aetiology of the disease[80,81].

The process of $(GV)_4$ aggregation in water mostly follows a two step condensation-ordering mechanism, however other pathways of water expulsion are observed. Disordered aggregate conformations are observed with poly-valine octapeptides in water, suggesting the influence of sequence patterning in ordered aggregation. Without dipolar interactions, the disordered aggregate does not rearrange into a fibril-like ordered conformation. . Therefore, a balance between hydrophobicity and dipolar interactions is needed to fold correctly[47], or to self assemble into fibril like aggregates. This balance was achieved while parameterizing WEPPROM[47], where too much or too less hydrophobicity resulted in collapsed or unfolded peptide conformations. The aggregation pathway in water exhibits two major off-pathway ordered aggregates, cross-β type and extended fibril-like structures. The extended fibril-like structure exhibits a water solvated hydrophobic face. The formation of the pseudo H-bond network in this structure compensates for the exposure of the hydrophobic groups to the water environment.

On comparison with aggregation at hydrophobic-hydrophilic interfaces, we observe that the presence of an interface (a) increases order in the final aggregate conformations, (b) decrease disordered conformations explored by the trajectory and (c) increases rate of aggregation; as the aggregates better align with the local electric field. On characterizing the angle between the dipole moment vectors and the local electric field for aggregates formed on the interface, a higher alignment of $\theta \approx 30 \pm 5^\circ$ is observed (compared to Figure S5b in water). When the interface is present, there is backbone dehydration, leading to more stronger dipole interactions, and hence better alignment with the local electric field. With the interface, there is less competition to form dipole-dipole interactions between backbone beads and the solvent which can introduce distortions into the pseudo H-bond network that can cause a decrease in order. The presence of a hydrophobic-hydrophilic interface also decreases the lag phase, or the time period before the formation of ordered aggregates. Also, the kinetics of aggregation is also more exponential or cooperative in nature when the interface is present. While fibril-like aggregates dominate conformations seen at the interface, cross-β-like conformations are more probable in the aqueous environment, however, fibril-like conformations in the aqueous environment is also observed. We see the formation of α-sheet like structures in all ordered fibril-like

Dipolar interactions play a crucial role in peptide aggregation, irrespective of environment. The presence of dipoles, both (a) stabilizes the aggregate and (b) induces order, which is made clear in this study by drawing comparisons between systems with and without dipolar particles. For peptides without dipolar particles, ordered aggregates are not observed in aqueous solvent and the peptides do not assemble or aggregate at the hydrophobic interface due to the lack of a driving force. The balance between hydrophobicity and dipolar interactions are different for aggregating peptides in water and at the hydrophobic interfaces. Hydrophobic interactions between peptides is lesser at the hydrophobic-hydrophilic interface, thus dipolar interactions play a more significant role in ordered aggregation at those interfaces. Our lab is currently working on studying other peptides, and membrane mediated peptide folding and aggregation.

5 Acknowledgements

This research was supported in part by the UMD-NCI Cancer Partnership for Cancer Technology and by the National Science Foundation under the Grant CHE-1454948 and through XSEDE resources provided by the Texas Advanced Computing Center (TACC) under the grant number TG-MCB120045.

References

1 D. Burdick, B. Soreghan, M. Kwon, J. Kosmoski, M. Knauer, A. Henschen, J. Yates, C. Cotman and C. Glabe, *J. Biol. Chem.*, 1992, **267**, 546–554.
2 E. Scherzinger, A. Sittler, K. Schweiger, V. Heiser, R. Lurz, R. Hasenbank, G. P. Bates, H. Lehrach and E. E. Wanker, *Proc. Natl. Acad. Sci. USA*, 1999, **96**, 4604–4609.
3 F. Chiti and C. M. Dobson, *Annu. Rev. Biochem.*, 2006, **75**, 333–366.
4 D. Thirumalai, D. Klimov and R. Dima, *Curr. Opin. Struct. Biol.*, 2003, **13**, 146–159.
5 M. Stefani and C. M. Dobson, *J. Mol. Med.*, 2003, **81**, 678–699.
6 C. M. Dobson, Semin. Cell Dev. Biol., 2004, pp. 3–16.
7 M. Fändrich, *Cell. Mol. Life Sci.*, 2007, **64**, 2066–2078.
8 S. B. Padrick and A. D. Miranker, *Biochemistry*, 2002, **41**, 4694–4703.
9 J. D. Harper and P. T. Lansbury Jr, *Annu. Rev. Biochem.*, 1997, **66**, 385–407.
10 T. R. Serio, A. G. Cashikar, A. S. Kowal, G. J. Sawicki, J. J. Moslehi, L. Serpell, M. F. Arnsdorf and S. L. Lindquist, *Science*, 2000, **289**, 1317–1321.
11 M. P. Lambert, A. Barlow, B. A. Chromy, C. Edwards, R. Freed, M. Liosatos, T. Morgan, I. Rozovsky, B. Trommer, K. L. Viola *et al.*, *Proc. Natl. Acad. Sci. USA*, 1998, **95**, 6448–6453.
12 N. Carulla, M. Zhou, M. Arimon, M. Gairí, E. Giralt, C. V. Robinson and C. M. Dobson, *Proc. Natl. Acad. Sci. USA*, 2009, **106**, 7828–7833.
13 C. Haass and D. J. Selkoe, *Nat. Rev. Mol. Cell Biol.*, 2007, **8**, 101–112.
14 S. Auer, F. Meersman, C. M. Dobson and M. Vendruscolo, *PLoS Comput. Biol.*, 2008, **4**, e1000222.
15 M. Zhu, P. O. Souillac, C. Ionescu-Zanetti, S. A. Carter and A. L. Fink, *J. Biol. Chem.*, 2002, **277**, 50914–50922.
16 R. Pellarin and A. Caflisch, *J. Mol. Biol.*, 2006, **360**, 882–892.
17 H. D. Nguyen and C. K. Hall, *Proc. Natl. Acad. Sci. USA*, 2004, **101**, 16180–16185.
18 B. Ma and R. Nussinov, *Curr. Opin. Chem. Biol.*, 2006, **10**, 445–452.
19 I. Kheterpal, S. Zhou, K. D. Cook and R. Wetzel, *Proc. Natl. Acad. Sci. USA*, 2000, **97**, 13597–13601.
20 D. J. Gordon and S. C. Meredith, *Biochemistry*, 2003, **42**, 475–485.
21 A. W. Fitzpatrick, T. P. Knowles, C. A. Waudby, M. Vendruscolo and C. M. Dobson, *PLoS Comput. Biol.*, 2011, **7**, e1002169.
22 S. Kumar, B. Ma, C.-J. Tsai, N. Sinha and R. Nussinov, *Prot. Sci.*, 2000, **9**, 10–19.
23 K. Tsemekhman, L. Goldschmidt, D. Eisenberg and D. Baker, *Prot. Sci.*, 2007, **16**, 761–764.
24 K. A. Burke, E. A. Yates and J. Legleiter, *Front Neurol*, 2013, **4**, 7.
25 A. Morriss-Andrews and J.-E. Shea, *J. Chem. Phys.*, 2012, **136**, 065103.
26 M. Y. Golovko, N. J. Faergeman, N. B. Cole, P. I. Castagnet, R. L. Nussbaum and E. J. Murphy, *Biochemistry*, 2005, **44**, 8251–8259.
27 S. Auer, C. M. Dobson and M. Vendruscolo, *HFSP J.*, 2007, **1**, 137–146.
28 S.-I. Kim, J.-S. Yi and Y.-G. Ko, *J. Cell. Biochem.*, 2006, **99**, 878–889.
29 R. Zahn, *J. Mol. Biol.*, 2003, **334**, 477–488.
30 S. Yu, S. Yin, N. Pham, P. Wong, S.-C. Kang, R. B. Petersen, C. Li and M.-S. Sy, *FEBS J.*, 2008, **275**, 5564–5575.
31 J. S. Capes, P. J. Kiley and A. H. Windle, *Langmuir*, 2010, **26**, 5637–5644.
32 A. Biswas, P. Kurkute, B. Jana, A. Laskar and S. Ghosh, *Chem. Commun.*, 2014, **50**, 2604–2607.
33 L. Fei and S. Perrett, *Prion*, 2010, **4**, 9–12.
34 R. M. Venable, Y. Zhang, B. J. Hardy and R. W. Pastor, *Science*, 1993, **262**, 223–226.
35 M. Seo, S. Rauscher, R. Pomès and D. P. Tieleman, *J. Chem. Theory Comput.*, 2012, **8**, 1774–1785.
36 A. Nikolic, S. Baud, S. Rauscher and R. Pomès, *Proteins*, 2011, **79**, 1–22.
37 N. V. Dokholyan, *Curr. Opin. Struct. Biol.*, 2006, **16**, 79–85.
38 R. L. Redler, D. Shirvanyants, O. Dagliyan, F. Ding, D. N. Kim, P. Kota, E. A. Proctor, S. Ramachandran, A. Tandon and N. V. Dokholyan, *J. Mol. Cell. Biol.*, 2014, **6**, 104–115.
39 A. Morriss-Andrews and J.-E. Shea, *Annu. Rev. Phys. Chem.*, 2015, **66**, 643–666.
40 G. Bitan, M. D. Kirkitadze, A. Lomakin, S. S. Vollers, G. B. Benedek and D. B. Teplow, *Proc. Natl. Acad. Sci. USA*, 2003, **100**, 330–335.
41 C. Wu and J.-E. Shea, *PLoS Comput. Biol.*, 2013, **9**, e1003211.
42 S. Abeln, M. Vendruscolo, C. M. Dobson and D. Frenkel, *PloS ONE*, 2014, **9**, e85185.
43 H. D. Nguyen and C. K. Hall, *Proc. Natl. Acad. Sci. USA*, 2004, **101**, 16180–16185.
44 R. Pellarin and A. Caflisch, *J. Mol. Biol.*, 2006, **360**, 882–892.
45 A. Morriss-Andrews, G. Bellesia and J.-E. Shea, *J. Chem. Phys.*, 2012, **137**, 145104.
46 G. Bellesia and J.-E. Shea, *J. Chem. Phys.*, 2009, **130**, 145103–145103.
47 S. J. Ganesan and S. Matysiak, *J. Chem. Theory Comput.*, 2014, **10**, 2569–2576.
48 S. J. Marrink, H. J. Risselada, S. Yefimov, D. P. Tieleman and A. H. de Vries, *J. Phys. Chem. B*, 2007, **111**, 7812–7824.
49 S. J. Grabowski, W. A. Sokalski and J. Leszczynski, *The Journal of Physical Chemistry A*, 2006, **110**, 4772–4779.
50 E. Isaacs, A. Shukla, P. Platzman, D. Hamann, B. Barbiellini and C. Tulk, *Journal of Physics and Chemistry of Solids*, 2000, **61**, 403–406.
51 H. S. Frank and W.-Y. Wen, *Discussions of the Faraday Society*, 1957, **24**, 133–140.
52 S. O. Yesylevskyy, L. V. Schäfer, D. Sengupta and S. J. Marrink, *PLoS Comput. Biol.*, 2010, **6**, e1000810.
53 B. Hess, C. Kutzner, D. Van Der Spoel and E. Lindahl, *J. Chem. Theory Comput.*, 2008, **4**, 435–447.
54 W. Humphrey, A. Dalke and K. Schulten, *J Mol Graph*, 1996, **14**, 33–38.
55 T. Darden, D. York and L. Pedersen, *J. Chem. Phys.*, 1993, **98**, 10089–10092.
56 B. Hess, H. Bekker, H. J. Berendsen, J. G. Fraaije *et al.*, *J. Comput. Chem.*, 1997, **18**, 1463–1472.
57 X. Sun and J. D. Gezelter, *J. Phys. Chem. B*, 2008, **112**, 1968–1975.
58 M. J. Stephen and J. P. Straley, *Rev. Mod. Phys.*, 1974, **46**, 617.
59 M. Cecchini, F. Rao, M. Seeber and A. Caflisch, *J. Chem. Phys.*, 2004, **121**, 10748–10756.
60 P. H. Nguyen, M. S. Li, G. Stock, J. E. Straub and D. Thirumalai, *Proc. Natl. Acad. Sci. USA*, 2007, **104**, 111–116.
61 V. A. Wagoner, M. Cheon, I. Chang and C. K. Hall, *Proteins*, 2014, **82**, 1469–1483.
62 R. Nelson, M. R. Sawaya, M. Balbirnie, A. Ø. Madsen, C. Riekel, R. Grothe and D. Eisenberg, *Nature*, 2005, **435**, 773–778.
63 D. R. Ripoll, J. A. Vila and H. A. Scheraga, *Proc. Natl. Acad. Sci. USA*, 2005, **102**, 7559–7564.
64 M. Cheon, I. Chang, S. Mohanty, L. M. Luheshi, C. M. Dobson, M. Vendruscolo and G. Favrin, *PLoS Comput. Biol.*, 2007, **3**, e173.
65 T. X. Hoang, A. Trovato, F. Seno, J. R. Banavar and A. Maritan, *Proc. Natl. Acad. Sci. USA*, 2004, **101**, 7960–7964.
66 D. Thirumalai, G. Reddy and J. E. Straub, *Acc. Chem. Res.*, 2011, **45**,

83–92.
67 N. L. Fawzi, E.-H. Yap, Y. Okabe, K. L. Kohlstedt, S. P. Brown and T. Head-Gordon, *Acc. Chem. Res.*, 2008, **41**, 1037–1047.
68 A. W. Fitzpatrick, G. T. Debelouchina, M. J. Bayro, D. K. Clare, M. A. Caporini, V. S. Bajaj, C. P. Jaroniec, L. Wang, V. Ladizhansky, S. A. Müller *et al.*, *Proc. Natl. Acad. Sci. USA*, 2013, **110**, 5468–5473.
69 M. Sunde, L. C. Serpell, M. Bartlam, P. E. Fraser, M. B. Pepys and C. C. Blake, *J. Mol. Biol.*, 1997, **273**, 729–739.
70 M. R. Sawaya, S. Sambashivan, R. Nelson, M. I. Ivanova, S. A. Sievers, M. I. Apostol, M. J. Thompson, M. Balbirnie, J. J. Wiltzius, H. T. McFarlane *et al.*, *Nature*, 2007, **447**, 453–457.
71 C. Aisenbrey, T. Borowik, R. Byström, M. Bokvist, F. Lindström, H. Misiak, M.-A. Sani and G. Gröbner, *Eur. Biophys. J*, 2008, **37**, 247–255.
72 H. M. Watkins, A. Vallée-Bélisle, F. Ricci, D. E. Makarov and K. W. Plaxco, *J. Am. Chem. Soc.*, 2012, **134**, 2120–2126.
73 L. Pauling and R. B. Corey, *Proc. Natl. Acad. Sci. USA*, 1951, **37**, 251–256.
74 V. Daggett, *Acc. Chem. Res.*, 2006, **39**, 594–602.
75 R. S. Armen, M. L. DeMarco, D. O. Alonso and V. Daggett, *Proc. Natl. Acad. Sci. USA*, 2004, **101**, 11622–11627.
76 G. W. Vandermeulen, K. T. Kim, Z. Wang and I. Manners, *Biomacromolecules*, 2006, **7**, 1005–1010.
77 M. Cheon, I. Chang and C. K. Hall, *Biophys. J.*, 2011, **101**, 2493–2501.
78 M. Cheon, I. Chang and C. K. Hall, *Protein Sci.*, 2012, **21**, 1514–1527.
79 J. Gsponer and M. Vendruscolo, *Protein Pept. Lett.*, 2006, **13**, 287–293.
80 Y.-R. Chen and C. G. Glabe, *J. Biol. Chem.*, 2006, **281**, 24414–24422.
81 S. L. Bernstein, N. F. Dupuis, N. D. Lazo, T. Wyttenbach, M. M. Condron, G. Bitan, D. B. Teplow, J.-E. Shea, B. T. Ruotolo, C. V. Robinson *et al.*, *Nat. Chem.*, 2009, **1**, 326–331.